Bioscience, Biotechnology, and Biochemistry, 2021, Vol. 85, No. 3, 611-620

doi: 10.1093/bbb/zbaa097
Advance access publication date: 13 February 2021
REGULAR PAPER

REGULAR PAPER

Metabolomic analysis to elucidate the change of the n-3 polyunsaturated fatty acids in senescent osteoblasts

Ying Wu,[1] Mengjun Zhang,[2] Xinwei Chen,[3] Yu Zhou,[1] and Zhou Chen [1,*]

[1]School of Pharmacy, Fujian Medical University, Fuzhou, Fujian, China; [2]Zhongshan Hospital, Fudan University (Xiamen Branch), Xiamen, Fujian, China; and [3]Graduation School of Fujian Medical University, Fuzhou, Fujian, China

*Correspondence: Zhou Chen, chenzhou@fjmu.edu.cn

ABSTRACT

Senile osteoporosis is a major public health concern, and yet, effective treatment methods do not exist. Herein, we used metabolomics to analyze the change of n-3 polyunsaturated fatty acids (PUFA) in senescent osteoblasts. We found that with an increase in the number of passages, the osteoblasts proliferative ability, alkaline phosphatase activity, and expression levels of bone metabolism genes decreased, the expression levels of aging-related genes increased, the damage caused by oxidative stress became more severe. Furthermore, levels of n-3 PUFA family members were downregulated in passage 10 than in passage 3 osteoblasts. These findings indicated that multiple passages led to more severe oxidative stress damage in senescent osteoblasts, which could be related to a decrease in n-3 PUFA levels. We believe that unsaturated fatty acid metabolism is a key factor involved in osteoblast senescence and that a proper dietary intake of n-3 PUFA may delay the occurrence senile osteoporosis.

Graphical Abstract

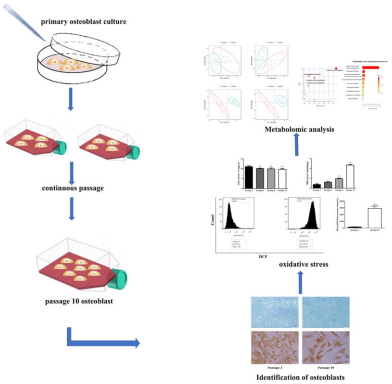

The change of n-3 PUFA in the senescent osteoblasts.

Received: 8 November 2020; **Accepted:** 17 November 2020

Keywords: senile osteoporosis, osteoblasts, oxidative stress, n-3 polyunsaturated fatty acids

Senile osteoporosis is an age-related metabolic bone disease caused by an imbalance between bone formation by osteoblasts and bone resorption by osteoclasts (Vilela and Nunes 2011; Kiernan, Davies and Stanford 2017). With a steady increase in the aging population, it has been estimated that >200 million people are currently suffering from osteoporosis worldwide (Aaseth, Boivin and Andersen 2012). It has thus become an important public health concern in elderly females as well as males considering the risk of consequent bone fractures, morbidity, disability, and socioeconomic costs (Heidari *et al.* 2017). Therefore, elucidating the mechanisms underlying senile osteoporosis and identifying potential markers of osteoporosis have become pivotal for reducing and preventing the occurrence of osteoporosis.

Age-related osteoblast dysfunction is believed to be the major cause of age-related bone loss in both men and women beyond the fifth decade (Lai *et al.* 2016). Targeting cellular senescence represents a novel therapeutic strategy to prevent bone loss (Khosla, Farr and Kirkland 2018). In our previous study, we found that primary cultured osteoblasts were closer in both form and function to senescent physiological conditions after continuous passaging, and in comparison to passage 3 osteoblasts, which served as a young control group, passage 10 osteoblasts served as the senescent model group (Zhang *et al.* 2019); moreover, oxidative stress level has been reported to be higher in passage 10 osteoblasts (Chen *et al.* 2019). Oxidative stress is an independent risk factor for the occurrence and development of osteoporosis (Wauquier *et al.* 2009). However, unfortunately, the detailed mechanism of oxidative stress in replicative senescence remains elusive.

Metabolomics is a highly recommended approach for studying "global" changes in metabolite profiles in a biological system (Zhao *et al.* 2018). Many recent metabolomic studies have examined which metabolites and specific metabolic pathways, such as energy, lipid, or amino acid metabolism pathways, are significantly altered during osteoporosis (Naylor and Eastell 2012; Nam *et al.* 2018). However, there still exists no sensitive and specific biomarker that can reflect the pathogenesis of senile osteoporosis *in vitro*. In this study, we characterized oxidative stress and other biological features of different passages of primary osteoblasts, obtained from Sprague–Dawley rats, that were continuously cultured *in vitro*; this was achieved by determining superoxide dismutase (SOD) activity, malondialdehyde (MDA) level, cell proliferative ability, alkaline phosphatase (ALP) activity, and bone metabolism and aging-related gene expression levels. Furthermore, we used metabolomics to identify the main metabolic signatures of serial passages so as to reveal the potential mechanisms underlying subculture senescence in osteoporosis.

Material and methods

Cell culture

Ethical approval for the use of animals in this study was granted by the Institutional Animal Care and Use Committee of Fujian Medical University (no. FJMU IACUC 2018-033). Primary osteoblasts were isolated from the calvaria of 8 newborn (<48 h) Sprague–Dawley male rats (Fujian Medical University Laboratory Animal Center, registration number: SCXK 2016-0002). Briefly, neonatal rat calvarias were dissected from the adherent soft tissue and periosteum and washed with PBS (Hyclone, USA) until the calvarias turned white. The tissue was sectioned into pieces of approximately 1 mm^3 and then sequentially digested with 3 mL 0.25% trypsin–EDTA (Genview, USA), followed by 4 mL 0.1% type I collagenase (Gibco, USA) mixed with 1 mL 0.25% trypsin–EDTA to release the cells. D-minimum essential medium (Hyclone, USA) was used for cell culture and was supplemented with 10% FBS (Hyclone, USA), L-glutamine (Beyotime, China), and penicillin–streptomycin (Genview, USA). The cells were seeded at a density of 5×10^5 cells/cm^2 in a T-25 flask and cultured overnight in an incubator with an atmosphere of 5% CO_2 at 37 °C. The cells were subcultured every 3- 4 days in fresh media, and those at passages 3, 6, 8, and 10 were chosen for subsequent experiments.

Identification of osteoblasts

Alkaline phosphatase staining

Osteoblasts were trypsinized and seeded onto slides. Alkaline phosphatase staining (Beijing Leagene Biotechnology, Beijing, China) was performed according to the manufacturer's protocol. In short, the cells were stained with methyl green for 3 min, washed with water, and then examined by microscopy.

SABC immunohistochemistry

Osteoblasts were trypsinized and seeded onto slides. SABC immunostaining (Boster Biological Technology Co. Ltd, Wuhan, China) was performed according to the manufacturer's protocol with a reaction time between 5 and 30 min. The samples were then washed in water and examined by microscopy.

Determination of cell viability

The cells belonging to the 4 groups (ie passage 3, 6, 8, and 10) were inoculated in a 96-well plate at a density of 3×10^3 cells/well. Each group included 5 replicates. After cell culture for 1 day and 5 days, 20 µL MTT (5 mg/mL, Sigma, USA) was added to each well, followed by incubation for 4 h. Subsequently, 100 µL of dimethyl sulfoxide (Sigma, USA) was added to each well, and the plate was oscillated for 10 min until the crystals completely dissolved. Optical density (OD) at 490 nm was measured using a microplate reader, and a blank control was included. The experiment was repeated at least 3 times.

Determination of ALP activity

The 4 groups of cells were inoculated in a 96-well plate at a density of 3×10^3 cells/well. Each group included 5 replicates. After cell culture for 5 days, 100 µL 0.1% Triton-X100 (Beijing Dingguo Changsheng Biotech, China) was added, and the plate was oscillated for 30 min until the cells were completely lysed. The cell lysates thus obtained were collected and stored at −80 °C. ALP activity was measured using an Alkaline Phosphatase Assay Kit (Beyotime, China), according to manufacturer instructions. OD at 405 nm was measured using a microplate reader, and a blank control was included. The experiment was repeated at least 3 times.

Quantitative real-time PCR

Total RNA was extracted using an RNA prep pure Cell/Bacteria Kit (Tiangen Biotech, China), according to manufacturer instructions. The concentration and purity of the isolated RNA samples were determined by measuring the absorbance at 260 and 280 nm. First-strand cDNA synthesis was then performed using 1 μg total RNA with a cDNA synthesis kit (DRR037A, TaKaRa, Japan). PCR primers (Table S1) were designed and synthesized by TaKaRa. Quantitative real-time PCR was performed using the Thermal Cycler Dice™ Real-Time System (Light Cycler, Roche). Briefly, 2 μL cDNA was included in a reaction volume of 25 μL, along with SYBR® Premix Ex Taq™ II (2×) (DRR081A, TaKaRa, Japan) and specific primers. All reactions were performed in triplicates, and data were analyzed using the $2^{-\Delta\Delta CT}$ method. β-Actin was used as the internal control, and the experiment was repeated at least 3 times.

Measure of reactive oxygen species by flow cytometry

A reactive oxygen species (ROS) Assay kit (Beyotime, China) was used for active ROS detection using the fluorescent probe 2′,7′-dichlorofluorescin diacetate (DCFH-DA). The osteoblasts were inoculated onto a 6-well plate at a density of 2×10^5 per well. DCFH-DA fluorescent probe was added into the cells using serum-free medium at a ratio of 1:1000 and placed in an incubator for 30 min, followed by washing of cells for 3 times and collection of cells. The cells were resuspended using the 200 μL serum-free medium. A flow cytometer (FACS Canto [TM] a) was used to quantify the relative fluorescence intensities.

Measurement of SOD activity and MDA accumulation

Oxidative stress refers to the imbalance between the production and eradication of ROS. SOD is the primary free-radical scavenger, and its activity is closely related to the degree of antioxidant stress. Moreover, MDA levels indicate the degree of lipid peroxidation and indirectly reflect the severity of cellular damage caused by free radicals. Thus, we herein chose SOD and MDA as the antioxidative marker and oxidative injury marker, respectively. The level of cellular SOD activity and MDA content was measured using corresponding assay kits (Nanjing Jiancheng Bioengineering Institute), according to manufacturer instructions.

Metabolomic analysis

Sample preparation

The cells at passage 3 and passage 10 were seeded at a density of $3 \times 10^5/cm^2$ in a 25-cm^2 T-flask for 5 days. After washing with PBS, the cells were scraped with a cell scraper and centrifuged at 1000 rpm and 4 °C for 5 min. PBS was then discarded, and the samples ($n = 6$/group) were snap-frozen in liquid nitrogen for 2 h and stored at −80 °C until needed.

The samples were thawed on ice, and metabolites were extracted with 50% methanol buffer. Briefly, 20 μL of a sample was extracted with 120 μL of precooled 50% methanol buffer, vortexed for 1 min, and incubated at room temperature for 10 min; the extraction mixture was then incubated overnight at −20 °C. After centrifugation at 4000 × *g* for 20 min, the supernatant was transferred into new 96-well plates. The samples were stored at −80 °C prior to LC–MS. In addition, pooled QC samples were obtained by combining 10 μL of each extraction mixture.

LC–QTOF/MS

LC–QTOF/MS was performed on an ultraperformance liquid chromatography (UPLC) system (SCIEX, UK) with a triple TOF™ 5600 plus mass spectrometer (SCIEX, UK). An ACQUITY UPLC T3 column (100 mm × 2.1 mm, 1.8 μm, Waters, UK) was used for chromatographic separation. All samples were analyzed in both positive and negative ion modes. Chromatographic conditions and MS parameters are listed in Supplementary Material.

Metabolite identification and processing

The acquired MS data pretreatments, including peak picking and grouping, retention time correction, second peak grouping, and annotation of isotopes and adducts, were performed using the XCMS software. LC–MS raw data files were converted into the mz.XML format and subsequently processed by the XCMS, CAMERA, and metaX toolbox implemented with the R software. Each ion was identified by combining retention time and *m/z* data. Intensities of each peaks were recorded and a three-dimensional matrix containing arbitrarily assigned peak indices (retention time–*m/z* pairs), sample names (observations), and ion intensity information (variables) was generated.

The online Kyoto Encyclopedia of Genes and Genomes (www.kegg.jp) database and human metabolome database (www.hmdb.ca) were used to annotate the metabolites by matching the exact molecular mass data (*m/z*) of samples with those in the database. Principal component analysis (PCA) was performed for outlier detection and batch effects evaluation using the preprocessed dataset. QC-based robust LOESS signal correction was fitted to the QC data with respect to the order of injection to minimize signal intensity drift over time. In addition, relative standard deviations of the metabolic features were calculated across all QC samples, and those >30% were removed. Student's *t*-test was used to detect differences in metabolite concentrations between the 2 phenotypes. *P* value was adjusted for multiple tests based on false discovery rate (Benjamini–Hochberg). Supervised partial least-squares discriminant analysis (PLS-DA) was conducted through metaX to discriminate different variables between the groups, and variable importance in projection (VIP) values were calculated. A VIP cutoff value of 1.0 was used to select key features.

Pathway and metabolite set enrichment analyses of significant biomarkers were performed with MetaboAnalyst 4.0 (www.metaboanalyst.ca) for the identification of top altered pathways and visualization. Over-representation analysis was performed using Fisher's exact test. Relative-betweenness centrality was used for pathway topology analyses.

Statistical analysis

Values are presented as mean ± SD. Statistical analyses were performed using SPSS version 20.0 (SPSS Inc., IBM, Somers, NY). One-way ANOVA was used for all group analyses, and pair-wise comparisons were analyzed with Tukey HSD. Differences were considered significant at a *P* value <.05.

Results

Identification of osteoblasts

Alkaline phosphatase activity is widely used as an indicator of osteoblast differentiation. Alkaline phosphatase-positive areas (indicated by blue staining) were observed in both the passage 3 and passage 10 osteoblasts (Figure 1a), indicating that the cultured cells produced alkaline phosphatase, which is characteristic of osteoblasts consistent. These observations indicate that the passage 3 and passage 10 cells are osteoblasts. The

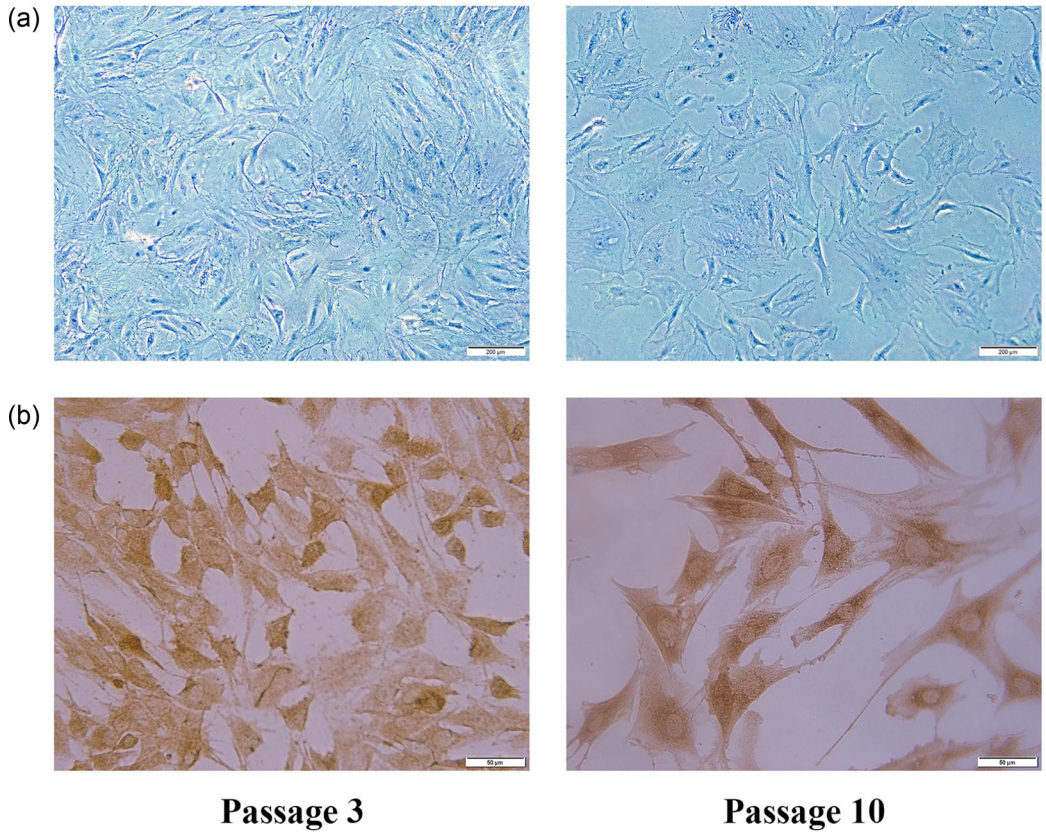

Figure 1. Identification of passage 3 and passage 10 osteoblasts. (a) Alkaline phosphatase staining of osteoblasts at passage 3 and passage 10, magnification 100×; (b) immunohistochemical staining for type-I collagen on primary osteoblasts at passage 3 and passage 10, magnification 100×.

extracted 2 groups of passage 3 and passage 10 cells showed brown type I collagenase staining, indicating that they were osteoblasts (Figure 1b). The cell body of the passage 10 osteoblast is larger than that of the passage 3 osteoblast, and the density of the passage 10 osteoblast is lower than that of the passage 3 osteoblast. Through counting, we found that the number of alkaline phosphatase staining positive cells and type I collagenase staining positive cells is greater than 95% of the total number of osteoblasts.

Detection of cell proliferative ability and ALP activity

MTT staining revealed that with an increase in the passage number of osteoblasts, the relative ratio of MTT gradually decreased. The cell viability of passage 6, 8, and 10 groups decreased significantly compared with passage 3 ($P < .001$), the passage 8 and 10 groups cell viability were statistically significant (Figure 2a, $P < .01$). These observations suggested that with an increase in the passage number, the cell viability of osteoblasts decreased.

As osteoblasts secrete ALP, the activity of ALP is representative of the activity of osteoblasts. We herein used the PNPP method to determine ALP activity. With an increase in the passage number of osteoblasts, ALP activity gradually decreased significantly compared with passage 3 (Figure 2b, $P < .001$). These results confirmed that ALP activity of primary osteoblasts decreased with an increase in the passage number.

p16, p21, and p53 are related to the cellular aging process. With an increase in the passage number of osteoblasts, the expression levels of these aging-related genes showed a gradual increase (Figure 2c-e). In comparison to passage 3 osteoblasts, passage 10 osteoblasts showed a significant increase in the expression levels of p16 ($P < .001$), p21 ($P < .001$), and p53 mRNA ($P < .01$).

mRNA expression levels of bone metabolism and aging-related genes

IGF-1, OPG, RANKL, and BGP are the most relevant bone metabolism genes in osteoblasts. The RANKL/OPG mRNA ratio plays a key role in the formation and absorption of the bone tissue. RANKL's binding to RANK on osteoclasts is regulated by osteoprotegerin (OPG), which is its soluble decoy receptor (Khera *et al.* 2019). With an increase in the passage number of osteoblasts, the expression levels of the aforementioned genes gradually declined (Figure 3a-d). In comparison to passage 3 osteoblasts, IGF-1, BGP, OPG, and RANKL mRNA expression levels in passage 10 osteoblasts decreased by 54.4%, 52.3%, 62.6%, and 54.9% (all $P < .01$), respectively; and the RANKL/OPG mRNA ratio showed an increase trend ($P = .084$).

The level of oxidative stress and mRNA expression levels of peroxisome proliferator-activated receptor-γ, peroxisome proliferator-activated receptor-α and FOXO1 in osteoblast

To evaluate oxidative stress damage, SOD activity, MDA accumulation and ROS levels were determined in 2 groups. We found that with an increase in osteoblast passages, SOD

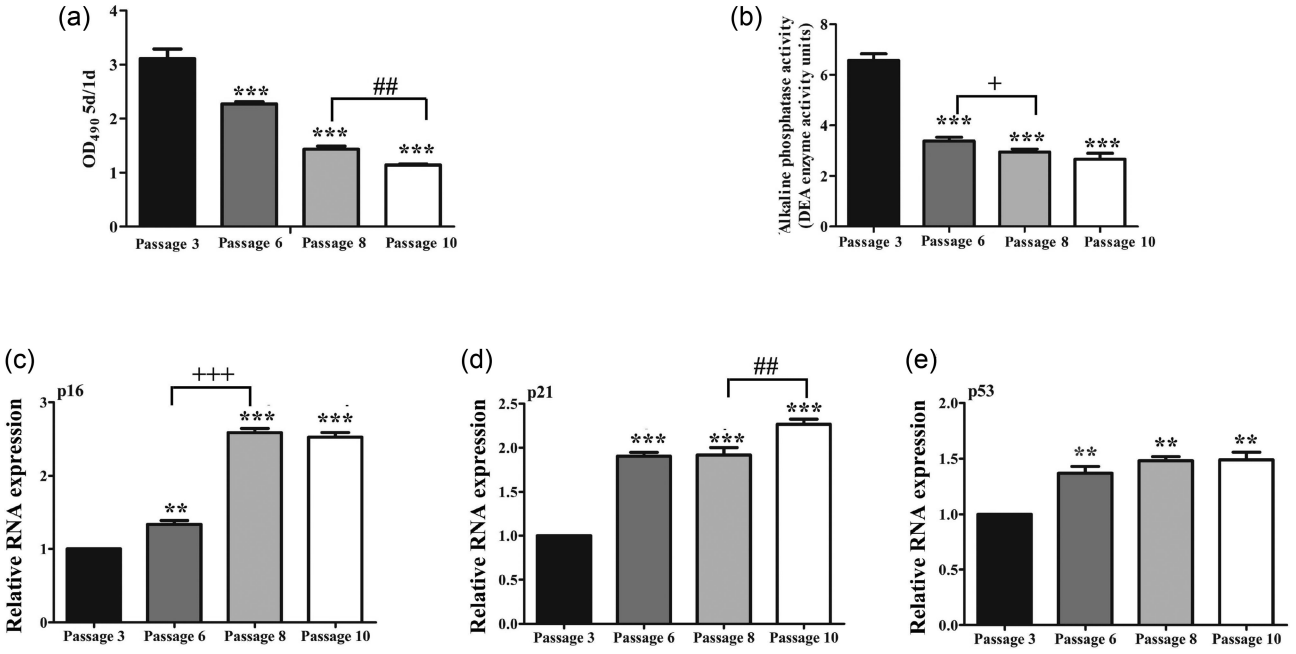

Figure 2. Cell proliferative ability, ALP activity, and expression levels of aging-related genes. (a) Proliferative ability of osteoblasts in different passages, (b) ALP activity of osteoblasts, and (c-e) Expression levels of p16, p21, and p53. $^{**}P < .01$, $^{***}P < .001$ compared to the passage 3 group; $^{+}P < .05$, $^{+++}P < .001$ compared to the passage 6; $^{\#\#}P < .01$ compared to the passage 8. Each experiment was performed in triplicate.

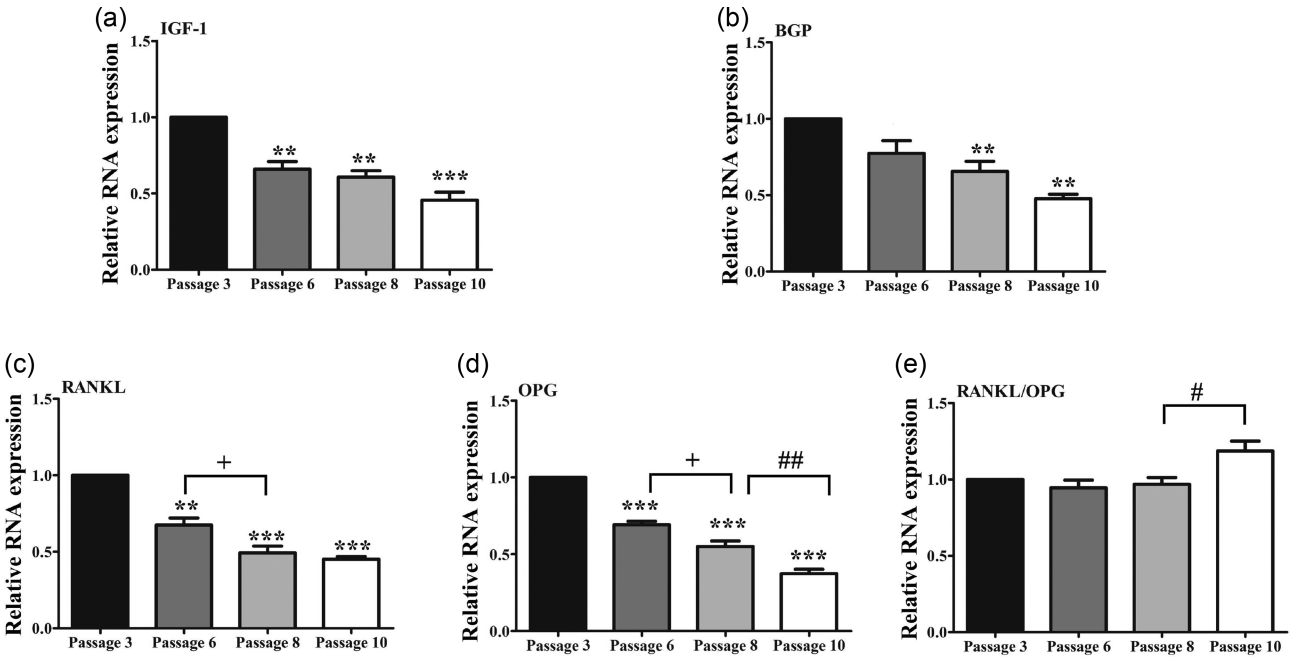

Figure 3. mRNA expression levels of bone metabolism genes. (a-d) mRNA expression levels of IGF-1, BPG, OPG, and RANKL, and (e) the RANKL/OPG mRNA ratio. $^{**}P < .01$, $^{***}P < .001$ compared to the passage 3 group; $^{+}P < .05$ compared to the passage 6; $^{\#}P < .05$ compared to the passage 8. Each experiment was performed in triplicate.

activity was inhibited (Figure 4a, $P < .05$), whereas MDA levels (Figure 4b) and ROS levels (Figure 4c) showed an obvious increase ($P < .001$). These results indicated that with an increase in the number of passages, damage due to oxidative stress became severe. The mRNA expression level of peroxisome proliferator-activated receptor-γ (PPAR-γ) (Figure 4d), peroxisome proliferator-activated receptor-α (PPAR-α) (Figure 4e) and FOXO1 (Figure 4f) in passage 3 was lower than that in passage 10 osteoblasts.

Metabolomic analysis

Data acquisition and identification of potential metabolic biomarkers

Our results revealed that after serial passages, cell proliferative ability, ALP activity, and expression levels of bone metabolism genes decreased, while the expression levels of aging-related genes increased. To determine how serial passages affect metabolic pathways, we analyzed the metabolomic profiles of passage 3 and 10 osteoblasts, obtaining a total of 5466 and 3182

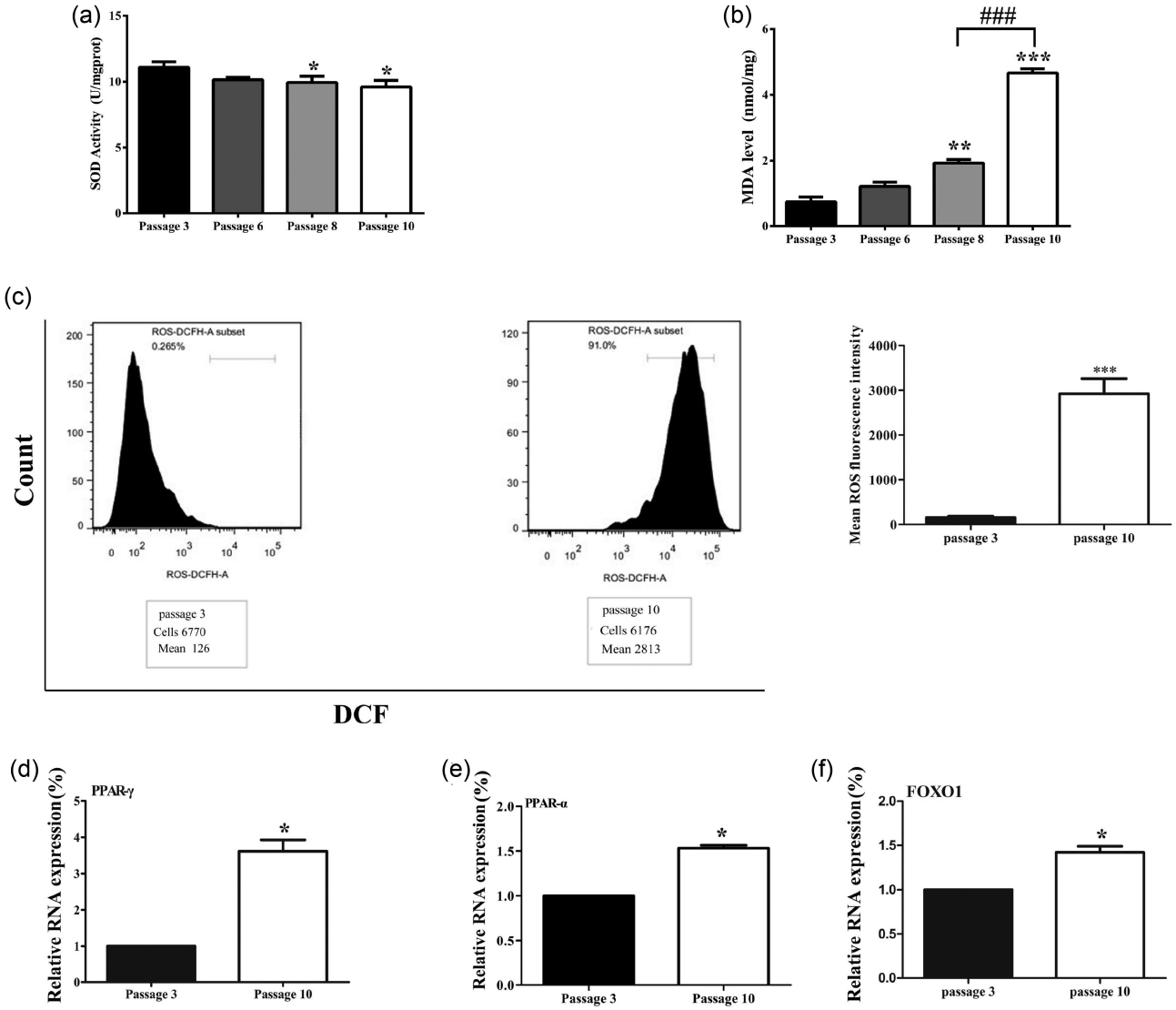

Figure 4. Detection of SOD activity, MDA accumulation, ROS, and mRNA expression levels of PPAR-γ, PPAR-α and FOXO1. (a) SOD activity, (b) MDA accumulation, (c) ROS levels, (d) mRNA expression levels of PPAR-γ, (e) mRNA expression levels of PPAR-α, (F) mRNA expression levels of FOXO1 $^{*}P < .05$, $^{**}P < .01$, $^{***}P < .001$ compared to the passage 3 group; $^{\#\#\#}P < .001$ compared to the passage 8. Each experiment was performed in triplicate.

aligned metabolite features detected by UPLC–QTOF–MS positive and negative ion modes, respectively.

The metabolic profile was plotted using PCA and PLS-DA, as shown in Figure 5. PCA was used for a comprehensive comparison between the groups, while PLS-DA was applied to maximize the difference of metabolic profiles and facilitate the detection of metabolites consistently present in the samples. PCA results indicated that in both the positive and negative ion modes, the score plot of the first two principal components (PC1 and PC2) revealed an indistinct distinction between the passage 3 and 10 groups (Figure 5a and b). We further analyzed the data pertaining to the 2 groups using a PLS-DA model. R^2 (defined as the proportion of variance in the data explained by the PLS-DA model and indicates goodness of fit) and Q^2 (defined as the proportion of variance in the data predicted by the PLS-DA model and indicates predictability) values indicated the quality of the PLS-DA model. Pronounced separations were observed between the passage 3 and 10 groups (Figure 5c and d), indicating their distinctly different metabolic profiles.

Altered lipid metabolites between the passage 3 and 10 groups

All identified metabolites satisfied the criteria (ie fold-change ≥ 2 or $< 1/2$, VIP values > 1 and P [Benjamini–Hochberg corrected] < 0.05), and they were considered to be differentially expressed between the passage 3 and 10 groups. We chose 37 metabolites belonging to the class "lipids and lipid-like molecules" and found that the levels of n-3 polyunsaturated fatty acid (PUFA) family showed a significant change (Table S2); for example, the levels of α-linolenic acid (ALA), docosahexaenoic acid (DHA), and eicosapentaenoic acid (EPA) were significantly lower in the passage 10 group than those in the passage 3 group. In comparison to the passage 3 group, the levels of few potential metabolites related to osteoporosis, such as kaurenic acid and methyltestosterone, were also lower in the passage 10 group. In the passage 10 group, members of the n-6 PUFA and n-9 PUFA families, such as arachidonic acid (AA), γ-linolenic acid (GLA), eicosenoic acid, and erucic acid, showed an upregulated expression level in comparison to that in the passage 3 group. We also witnessed an increase

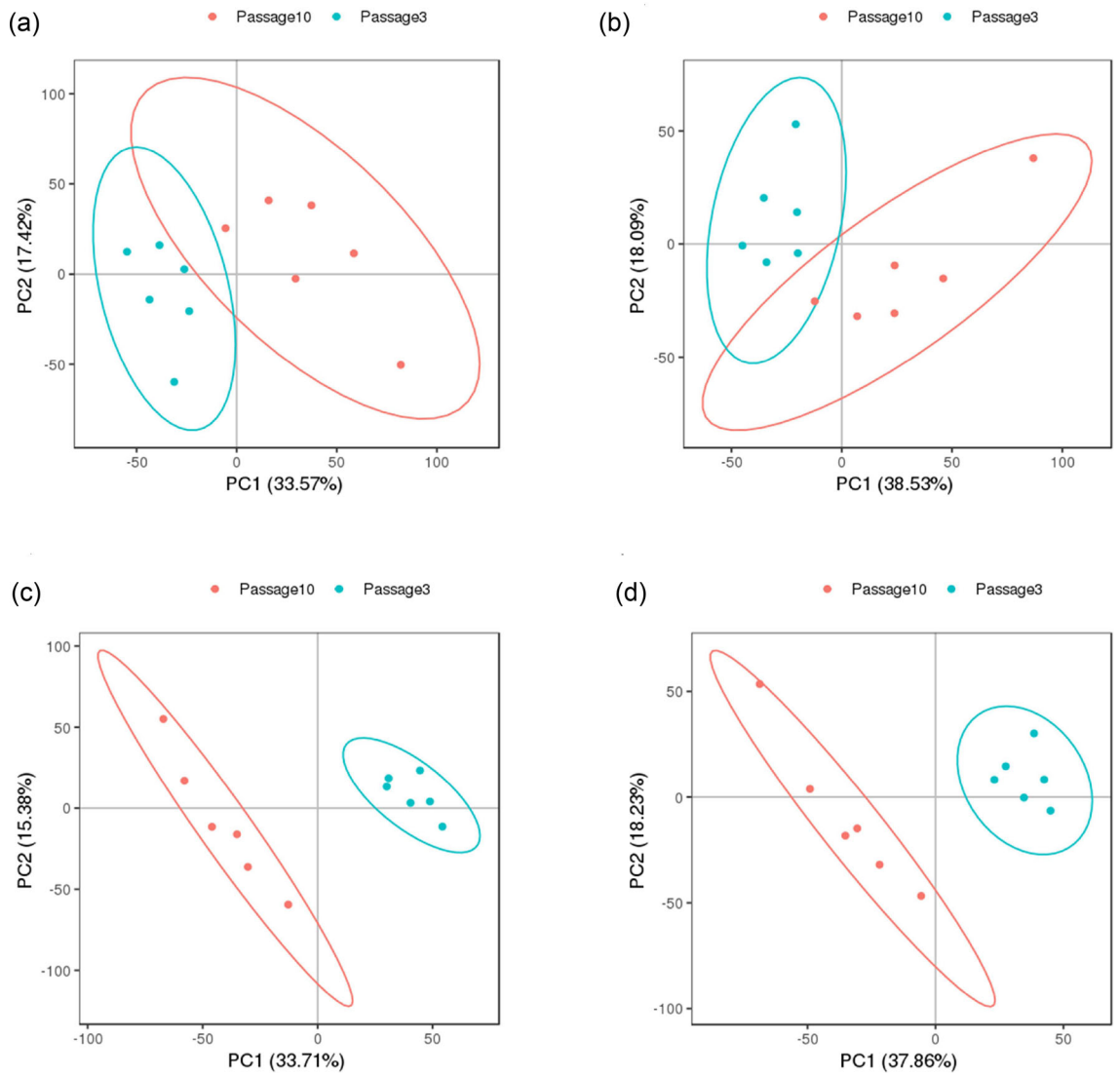

Figure 5. Multivariate statistical analysis of osteoblasts belonging to the passage 3 and 10 groups. Principal component analysis score plots of metabolites in the (a) positive and (b) negative ion mode of LC–MS; PLS-DA score plots from the spectra of the (c) positive ($R^2 = 0.985$, $Q^2 = 0.812$) and (d) negative ($R^2 = 0.968$, $Q^2 = 0.851$) ion mode of LC–MS.

in lysophosphatidylcholine and lysophosphatidylethanolamine levels in the passage 10 group than that in the passage 3 group.

The 37 significant biomarkers were subjected to pathway and enrichment analysis through MetaboAnalyst 4.0; Figure 6a shows the relevant metabolic pathways. The pathway impact value calculated from pathway topology analysis above 0.1 was filtered out as potential target pathway. Linoleic acid metabolism, sphingolipid metabolism, and ALA metabolism were the most important metabolic pathways affected by the serial passages. All 3 of these pathways are involved in lipid metabolism, suggesting that unsaturated fatty acid metabolism plays a major role in osteoblast senescence. Metabolite set enrichment analyses (Figure 6b) indicated that ALA and linoleic acid metabolism were the most affected by the serial passages, and these findings further confirmed that unsaturated fatty acid metabolism plays a key role in osteoblast senescence.

Discussion

Herein, we report that the senescent features and metabolomic profiles of primary osteoblasts substantially varied with the number of passages. We observed that with an increase in the passage number, osteoblasts showed lower cell viability, ALP activity, SOD and FOXO1 gene, as well as downregulated expression levels of bone metabolism genes; however, the expression levels of aging-related genes were upregulated and MDA levels and ROS levels were higher too. Moreover, the novel differentially expressed metabolic markers highlighted the importance of PUFA metabolism in the serial passage of primary osteoblasts, and this finding is in accordance with that observed in aged osteoporotic mice (Nam *et al.* 2018). The primary osteoblasts were closer in both form and function to senescent physiological conditions; and there are no studies showing the relationship between senescent osteoblasts and PUFA *in vitro*. In this experiment, we revealed the change of n-3 PUFA in

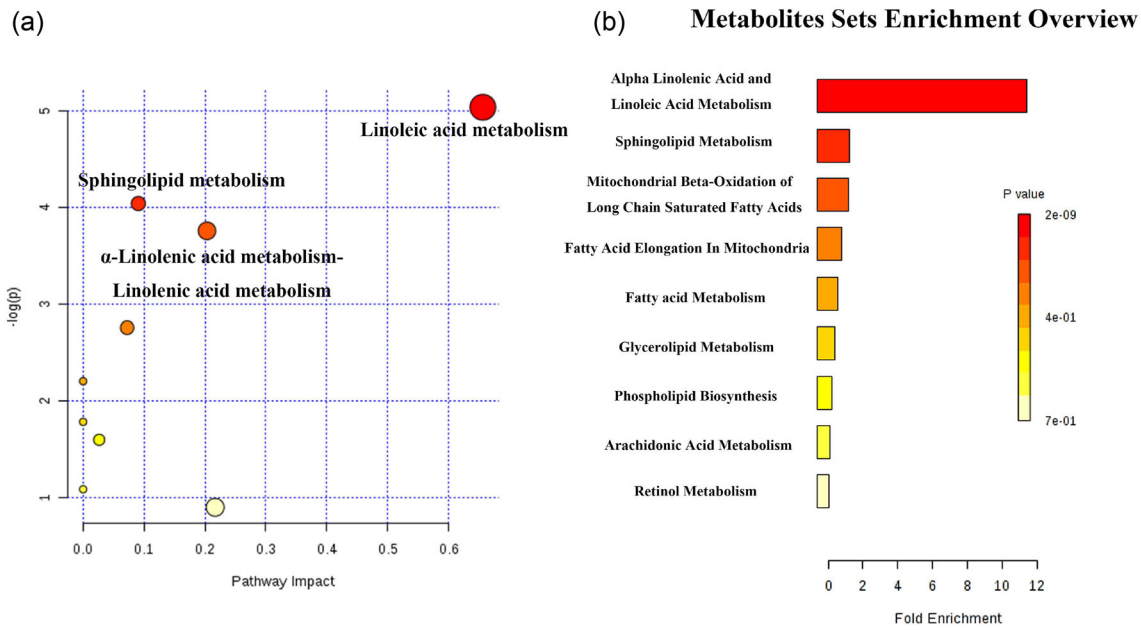

Figure 6. Pathway and enrichment analysis with MetaboAnalyst. (a) Pathway impact and (b) metabolite set enrichment overview.

senescent osteoblasts; for the related studies of polyunsaturated fatty acids in osteoporosis, most of the cell models are MC3T3-E1 osteoblast-like cells and the bone marrow MSC (Watkins *et al.* 2003; Casado-Díaz *et al.* 2014). In this study, we used successively passaged primary osteoblasts as the object to study the changes in polyunsaturated fatty acids, which has not been reported before in previous studies.

Our findings pertaining to the decrease in cell viability, ALP activity, and expression levels of bone metabolism genes with an increase in the passage number are consistent with those of Yu *et al.* (Mingxiang, Jin and Shuzhu 2002; Ming-Xiang *et al.* 2007) and Kveiborg *et al.* (2000, 2001). Yu *et al.* compared the characteristics between serially passaged cultures of osteoblasts of ≤5-year-old donors and osteoblasts of ≥70-year-old donors, and their results indicated that cell activity and expression levels of bone metabolism genes decreased with an increase in the passage number. However, the disadvantages of their research model were that the human bone is difficult to obtain, the growth of primary cultured human osteoblasts is slow, and the experimental cycle is long; therefore, the application of such a model is limited. In this study, we used primary rat osteoblasts to establish an *in vitro* model. The RANKL/OPG mRNA ratio has a key role in bone resorption and bone formation, and it is thus widely used to determine bone remodeling ability. Activated RANKL is related to RANK, which excites on the osteoclasts for bone resorption. OPG is an antiresorptive agent that acts as a decoy receptor for RANKL (Tousen *et al.* 2020). Our results showed that the difference between passage 3 and passage 6 or 8 was not statistically significant. In contrast, at passage 10, the ratio increased, suggesting a stronger ability of osteoblasts to promote osteoclast differentiation. With respect to cell senescence, we chose the following aging-related genes: p16, p21, and p53. We found that the passage 8 and 10 groups showed no significant differences in p53 and p16 mRNA expression levels. It is reasonable to speculate that from passage 8 onward, osteoblasts would have entered the state of senescence. We attempted to subculture the cells until passage 13, but the incubation time significantly increased, cell vitality considerably decreased, frequency of cell death increased, and cell count markedly decreased. Therefore, we propose that using passage 10 osteoblasts is ideal for studying senile osteoporosis.

It is recognized that lipid metabolism has a close relationship with bone metabolism (Cui *et al.* 2005). Bone and fat cells share a common progenitor, namely multipotent mesenchymal stem cells (MSCs) within the bone marrow (BM); therefore, lipid and bone metabolism are evidently interrelated (Tian and Yu 2015). Several large observational studies have highlighted a positive association between the higher dietary intake of n-3 PUFA and a decreased risk of fractures or an increase in total body, femur, or lumbar spine bone mineral density in postmenopausal women (Longo and Ward 2016). Similarly, the positive influence of the dietary intake of n-3 PUFA on bone mineral density, bone mineral content, and bone calcium levels has been reported in elderly men (Hogstrom, Nordstrom and Nordström 2007; Mangano *et al.* 2014). Our results confirmed that levels of ALA, DHA, and EPA (members of the n-3 PUFA family) significantly decreased in the passage 10 group in comparison to those in the passage 3 group. Moreover, the expression levels n-6 PUFA family members were downregulated, while those of saturated fatty acids, such as arachidic acid, were upregulated. These differentially expressed metabolites were involved in several metabolic pathways, such as linoleic acid metabolism, sphingolipid metabolism, and ALA metabolism.

Alterations in the levels of lipid metabolites have been associated with oxidative stress. The impairment of lipid on bone is due to ROS formation by saturated fatty acid peroxidation (Cnop *et al.* 2001). Increased free saturated fatty acid levels enhance ROS production, and ROS accumulation can lead to lipotoxicity (Pino and Rodríguez 2017). On the contrary, unsaturated fatty acids, particularly n-3 PUFA, have been reported to have a protective effect on the bone as they promote osteogenesis (Wauquier *et al.* 2012). This could be attributed to the antioxidant effects of n-3 PUFA (Umesha and Naidu 2015). In the present study, in comparison with passage 3 osteoblasts, the damage caused by oxidative stress was severe in passage 10 osteoblasts, as indicated by a decrease in SOD activity and an increase in MDA levels and ROS levels. Moreover, the expression levels of PPAR-γ and PPAR-α were upregulated in the passage 10 group. PPAR-γ is an essential

regulator of adipocyte differentiation, and it may determine the differentiation direction of bone marrow stromal cells into osteoblasts or adipocytes (Ge *et al.* 2016). Oxidized lipids, acting as the ligands of PPAR-γ, promote the binding of PPAR-γ, and adipogenesis requires the activation of the nuclear hormone receptor PPAR-γ; these changes reportedly coincide with a rise in oxidative stress and a decrease in osteoblast count (Almeida *et al.* 2009). PPAR-α is a nuclear/transcription receptor/factor that regulates lipid metabolism, stimulation of PPAR-α triggers uptake, and utilization and catabolism of FAs via the upregulation of genes associated with FA transport and peroxisomal and mitochondrial β-oxidation (Nakamura, Yudell and Loor 2014). Therefore, we hypothesize that after 10 osteoblast passages, the increase of PPARα content in the passage 10 osteoblasts may lead to a decrease in the content of n-3 PUFA, which made more saturated fatty acid produced. Saturated fatty acid connected with PPARγ further leads to the development of senile osteoporosis. These results confirm our previous hypothesis that oxidative stress in continuous passage of osteoblasts is associated with lipid metabolism. In agreement with our observation, Almeida *et al.* (2009) reported that altered lipid metabolism causes oxidative stress and upregulation of PPAR-γ, which reduces osteoblast number in the skeleton.

Insulin/IGF-1 signaling pathway influences cell senescence (Kenyon 2010). In previous studies, we have demonstrated that the IGF-1/PI3K/AKT signaling pathway is significantly downregulated in passage 10 osteoblasts (Chen *et al.* 2019), which may inhibit the activity of the transcriptional activity of FOXO1. Oxidative stress changes mediated by the accumulation of reactive oxygen species (ROS) lead to a significant increase in the transcriptional activity of FOXO1 (Tiwari *et al.* 2016), which is consistent with what we found in senescent osteoblasts. In this study, compared with passage 3, we found that the expression level of FOXO1 mRNA expression increased 1.43-folds in the passage 10 osteoblast.

To summarize, our findings suggest that primary osteoblasts from Sprague–Dawley rats after serial passages *in vitro* mimic the physiological state of the living bone tissue. Herein, we determined the cell proliferative ability, ALP activity, expression levels of bone metabolism and aging-related genes, SOD activity, MDA accumulation, ROS levels and FOXO1 mRNA level, and we report that passage 10 osteoblasts were used to establish a robust cell model for studying senile osteoporosis. In addition, our metabolomic analyses revealed that the decrease in n-3 PUFA levels in senescent osteoblasts may aggravate the damage due to oxidative stress and the expression levels of PPAR-γ and PPAR-α. We also report that unsaturated fatty acid metabolism is a significant factor involved in osteoblast senescence and that a proper dietary intake of n-3 PUFA (EPA and DHA) may delay the occurrence senile osteoporosis; however, further studies are warranted to confirm our observations.

Supplementary material

Supplementary material is available at *Bioscience, Biotechnology, and Biochemistry* online.

Author Contribution

Zhou Chen and Ying Wu designed the study; Ying Wu guided the experiment. Xin-wei Chen and Meng-jun Zhang performed the research; Meng-jun Zhang and Xin-wei Chen analyzed the data and wrote the paper; Yu Zhou revised the paper.

Funding

This study was supported by the Fourth Round of Fujian Provincial Joint Tackling Project between Health and Education Joint Research Fund of National Health and Family Planning Commission of China (WKJ2016-2-02).

Disclosure statement

No potential conflict of interest was reported by the authors.

References

Aaseth J, Boivin G, Andersen O. Osteoporosis and trace elements—an overview. *J Trace Elem Med Biol* 2012;**26**:149-52.

Almeida M, Ambrogini E, Han L *et al.* Increased lipid oxidation causes oxidative stress, increased peroxisome proliferator-activated receptor-gamma expression, and diminished pro-osteogenic Wnt signaling in the skeleton. *J Biol Chem* 2009;**284**:27438-48.

Casado-Díaz A, Ferreiro-Vera C, Priego-Capote F *et al.* Effects of arachidonic acid on the concentration of hydroxyeicosatetraenoic acids in culture media of mesenchymal stromal cells differentiating into adipocytes or osteoblasts. *Genes Nutr* 2014;**9**:375.

Chen X, Li YH, Zhang MJ *et al.* Lactoferrin ameliorates aging-suppressed osteogenesis via IGF1 signaling. *J Mol Endocrinol* 2019;**63**:63-75.

Cnop M, Hannaert JC, Hoorens A *et al.* Inverse relationship between cytotoxicity of free fatty acids in pancreatic islet cells and cellular triglyceride accumulation. *Diabetes* 2001;**50**:1771-7.

Cui LH, Shin MH, Chung EK *et al.* Association between bone mineral densities and serum lipid profiles of pre- and postmenopausal rural women in South Korea. *Osteoporos Int* 2005;**16**:1975-81.

Ge C, Cawthorn WP, Li Y *et al.* Reciprocal control of osteogenic and adipogenic differentiation by ERK/MAP kinase phosphorylation of Runx2 and PPARgamma transcription factors. *J Cell Physiol* 2016;**231**:587-96.

Heidari B, Muhammadi A, Javadian Y *et al.* Associated factors of bone mineral density and osteoporosis in elderly males. *Int J Endocrinol Metab* 2017;**15**:e39662.

Hogstrom M, Nordstrom P, Nordström A. n-3 Fatty acids are positively associated with peak bone mineral density and bone accrual in healthy men: the NO_2 study. *Am J Clin Nutr* 2007;**85**:803-7.

Kenyon CJ. The genetics of ageing. *Nature* 2010;**464**:504-12.

Khera A, Kanta P, Kalra J *et al.* Resveratrol restores the level of key inflammatory cytokines and RANKL/OPG ratio in the femur of rat osteoporosis model. *J Women Aging* 2019;**31**:540-52.

Khosla S, Farr JN, Kirkland JL. Inhibiting cellular senescence: a new therapeutic paradigm for age-related osteoporosis. *J Clin Endocrinol Metab* 2018;**103**:1282-90.

Kiernan J, Davies JE, Stanford WL. Concise review: musculoskeletal stem cells to treat age-related osteoporosis. *Stem Cells Transl Med* 2017;**6**:1930-9.

Kveiborg M, Flyvbjerg A, Rattan SIS *et al.* Changes in the insulin-like growth factor-system may contribute to in vitro age-related impaired osteoblast functions. *Exp Gerontol* 2000;**35**:1061-74.

Kveiborg M, Rattan SI, Clark BF *et al.* Treatment with 1,25-dihydroxyvitamin D3 reduces impairment of human osteoblast functions during cellular aging in culture. *J Cell Physiol* 2001;**186**:298-306.

Lai P, Song Q, Yang C *et al*. Loss of Rictor with aging in osteoblasts promotes age-related bone loss. *Cell Death Dis* 2016;**7**:e2408.

Longo AB, Ward WE. Providing flaxseed oil but not menhaden oil protects against OVX induced bone loss in the mandible of Sprague–Dawley rats. *Nutrients* 2016;**8**: 597.

Mangano KM, Kerstetter JE, Kenny AM *et al*. An investigation of the association between omega 3 FA and bone mineral density among older adults: results from the National Health and Nutrition Examination Survey years 2005–2008. *Osteoporos Int* 2014;**25**:1033-41.

Mingxiang YU, Jin W, Shuzhu GU. Influence of increasing donor age on human osteoblastic cells cultured in vitro. *Chin J Endocrinol Metabol* 2002;**2**:116-19.

Ming-Xiang YU, Wang HF, Jin WF *et al*. Comparison of biology characteristics between infant human osteoblasts of subculture senescence and ≥70 year-old human osteoblasts in vitro. *Fudan Univ J Med Sci* 2007;**34**:42-6.

Nakamura MT, Yudell BE, Loor JJ. Regulation of energy metabolism by long-chain fatty acids. *Prog Lipid Res* 2014; **53**:124-44.

Nam M, Huh JE, Kim MS *et al*. Metabolic alterations in the bone tissues of aged osteoporotic mice. *Sci Rep* 2018;**8**:8127.

Naylor K, Eastell R. Bone turnover markers: use in osteoporosis. *Nat Rev Rheumatol* 2012;**8**:379-89.

Pino AM, Rodríguez JP. Is fatty acid composition of human bone marrow significant to bone health? *Bone* 2017;**118**:53-61.

Tian L, Yu X. Lipid metabolism disorders and bone dysfunction–interrelated and mutually regulated (review). *Mol Med Rep* 2015;**12**:783-94.

Tiwari HS, Misra UK, Kalita J *et al*. Oxidative stress and glutamate excitotoxicity contribute to apoptosis in cerebral venous sinus thrombosis. *Neurochem Int* 2016;**100**: 91-6.

Tousen Y, Ichimaru R, Kondo T *et al*. The combination of soy isoflavones and resveratrol preserve bone mineral density in hindlimb-unloaded mice. *Nutrients* 2020;**12**:2043.

Umesha SS, Naidu KA. Antioxidants and antioxidant enzymes status of rats fed on n-3 PUFA rich Garden cress (Lepidium Sativum L) seed oil and its blended oils. *J Food Sci Technol* 2015;**52**:1993-2002.

Vilela P, Nunes T. Osteoporosis. *Neuroradiology* 2011;**53**: 185-9.

Watkins BA, Li Y, Lippman HE *et al*. Modulatory effect of omega-3 polyunsaturated fatty acids on osteoblast function and bone metabolism. *Prostaglandins Leukot Essent Fatty Acids* 2003;**68**:387-98.

Wauquier F, Barquissau V, Léotoing L *et al*. Borage and fish oils lifelong supplementation decreases inflammation and improves bone health in a murine model of senile osteoporosis. *Bone* 2012;**50**:553-61.

Wauquier F, Leotoing L, Coxam V *et al*. Oxidative stress in bone remodelling and disease. *Trends Mol Med* 2009;**15**:468-77.

Zhang M, Xie Y, Zhou Y *et al*. Exendin-4 enhances proliferation of senescent osteoblasts through activation of the IGF-1/IGF-1R signaling pathway. *Biochem Biophys Res Commun* 2019;**516**: 300-6.

Zhao Q, Shen H, Su KJ *et al*. Metabolomic profiles associated with bone mineral density in US Caucasian women. *Nutr Metab* 2018;**15**:57.